Journal of Energy Chemistry 52 (2021) 115–120

Contents lists available at ScienceDirect

Journal of Energy Chemistry

journal homepage: www.elsevier.com/locate/jechem

http://www.journals.elsevier.com/journal-of-energy-chemistry/

Chlorine-anion doping induced multi-factor optimization in perovskties for boosting intrinsic oxygen evolution

Yinlong Zhu[a,1,*], Qian Lin[a,1], Zhenbin Wang[b], Dongchen Qi[c], Yichun Yin[a], Yu Liu[d], Xiwang Zhang[a], Zongping Shao[d], Huanting Wang[a]

[a] Department of Chemical Engineering, Monash University, Clayton, VIC 3800, Australia
[b] Department of Physics, Technical University of Denmark, 2800 Kongens Lyngby, Denmark
[c] School of Chemistry and Physics, Centre for Materials Science, Queensland University of Technology, Brisbane, Queensland 4001, Australia
[d] Department of Chemical Engineering, Curtin University, Perth, Western Australia 6845, Australia

ARTICLE INFO

Article history:
Received 17 March 2020
Revised 27 March 2020
Accepted 30 March 2020
Available online 25 April 2020

Keywords:
Anion doping
Halogen chlorine
Multiple beneficial factors
Oxygen evolution reaction
Perovskite oxide

ABSTRACT

The oxygen evolution reaction (OER) plays a crucial role in many electrochemical energy technologies, and creating multiple beneficial factors for OER catalysis is desirable for achieving high catalytic efficiency. Here, we highlight a new halogen-chlorine (Cl)-anion doping strategy to boost the OER activity of perovskite oxides. As a proof-of-concept, proper Cl doping at the oxygen site of $LaFeO_3$ (LFO) perovskite can induce multiple favorable characteristics for catalyzing the OER, including rich oxygen vacancies, increased electrical conductivity and enhanced Fe-O covalency. Benefiting from these factors, the $LaFeO_{2.9-\delta}Cl_{0.1}$ (LFOCl) perovskite displays significant intrinsic activity enhancement by a factor of around three relative to its parent LFO. This work uncovers the effect of Cl-anion doping in perovskites on promoting OER performance and paves a new way to design highly efficient electrocatalysts.

1. Introduction

Due to ever-increasing energy demand and environmental pollution worldwide, substantial research has been devoted to the development of sustainable energy technologies [1]. The electrochemical oxygen evolution reaction (OER), a key half reaction in multiple clean energy technologies (i.e., water splitting, metal-air batteries and CO_2/N_2 electrolysis), is the bottleneck of these processes on account of its sluggish kinetics involving multistep electron transfers [2–6]. Currently, noble metal oxides of ruthenium (Ru)/iridium (Ir) are deemed as the state-of-the-art OER electrocatalysts with low overpotentials, but their scarcity and high price impeded the wide-scale practical application [6,7]. Therefore, great efforts have been dedicated to exploit efficient and low-cost noble-metal-free electrocatalysts for OER.

Among various alternatives, non-noble perovskite oxides have received extensive interest in the OER electrocatalysis by virtue of their flexible composition and structure for tuning catalytic activity [8–15]. $LaFeO_3$, a representative parent oxide in the family of perovskite, has gained various application in catalysis, sensors, water treatment and solid oxide fuel cells, etc. [16–20]; however, it has poor OER activity [8,21,22]. To overcome this dilemma, a few approaches have been made [23–28]. Doping of A- or B-site cations is an effective way to enhance OER activity [25–28]. For example, She et al. conducted a detailed study of Sr-doped $La_{1-x}Sr_xFeO_{3-\delta}$ perovskites and found A-site Sr-doping results in distinct activity enhancement [26]. The OER activity of $LaFeO_3$ could be also improved by proper B-site Co-ion doping [27]. Moreover, Liu's group achieved the enhanced electrocatalytic OER activity by non-metal P^{5+} doping into the $LaFeO_3$ perovskite [28]. Thus, cationic doping has been recognized as a mature method for regulating the catalytic activity.

In addition to the traditional cationic doping strategy, it has been reported that the doping of partial non-oxygen anions at the oxygen sites could sometimes generate several interesting properties and thereby promote catalytic performance [29–38]. For instance, fluorine (F)-anion doping into $SrCoO_{3-\delta}$, $Ba_{0.5}Sr_{0.5}Co_{0.8}Fe_{0.2}O_{3-\delta}$ and $La_{0.5}Ba_{0.25}Sr_{0.25}CoO_{3-\delta}$ perovskites enables an evident improvement in the OER activity [29–31]. Some F-doped perovskite oxides were also developed as efficient catalysts for high-temperature electrochemical energy devices, such as solid oxide fuel cells, solid oxide electrolysis cells and oxygen permeation membrane [32–34]. Besides, Peng et al. proposed that sul-

---

* Corresponding author.
E-mail addresses: yinlong.zhu@monash.edu (Y. Zhu), huanting.wang@monash.edu (H. Wang).

[1] These authors contributed equally to this work.

https://doi.org/10.1016/j.jechem.2020.03.055

fur (S) anion could be incorporated into the oxygen site of $CaMnO_3$ for boosting the bifunctional oxygen electrocatalysis performance [35]. Lower electronegativity of halogen chlorine (Cl) over oxygen (O) could lead to enhanced metal-oxygen covalent nature, which is beneficial for charge transfer during electrocatalysis process. However, up to now, little attention has been given to the Cl doped perovskites as efficient OER catalysts.

Inspired by above considerations, herein, we report an effective strategy for enhancing the OER electrocatalytic activity of $LaFeO_3$ (LFO) perovskite by simple Cl-anion doping. Remarkably, $LaFeO_{2.9-\delta}Cl_{0.1}$ (LFOCl, with ~3.3 at% Cl dopant at oxygen site) exhibits ~ 3-fold higher intrinsic activity than the parent LFO, along with a small Tafel slope of 59 mV dec^{-1}. The enhanced intrinsic activity of LFOCl could be ascribed to unique Cl-anion doping, which brings about multiple beneficial factors for OER catalysis, e.g., rich oxygen vacancies, increased electrical conductivity and enhanced metal-oxygen covalency.

2. Experimental

2.1. Catalyst synthesis

$LaFeO_{3-x-\delta}Cl_x$ ($x = 0$, 0.05, 0.1, 0.2) perovskites were synthesized by a combined ethylenediaminetetraacetic acid-citric acid (EDTA-CA) complexing sol-gel method. Taking the synthesis of $LaFeO_{2.9-\delta}Cl_{0.1}$ (LFOCl) as an example, stoichiometric amounts of $La(NO_3)_3•6H_2O$, $Fe(NO_3)_3•9H_2O$ and $LaCl_3•7H_2O$ were mixed in deionized water. The amount of Cl dopant in the LFOCl was tailored by the ratio of $LaCl_3•7H_2O$ to $La(NO_3)_3•6H_2O$ applied in the raw materials. EDTA and citric acid were then added as complexing agents in sequence at a mole ratio of 1:1:2 for total metal ions/EDTA/citric acid. To ensure complete complexation, the pH of the solution was adjusted to 6–7 by the addition of NH_3 aqueous solution. A transparent gel was obtained by heating at 90 °C under stirring. The gel was then heated in the furnace at 250 °C for 5 h in air to form a solid precursor. Finally, the solid precursor was calcined at 800 °C for 5 h in air to form LFOCl powder. The commercial IrO_2 powder was purchased from Aladdin Industrial Corporation.

2.2. Characterization

XRD patterns were collected using an X-ray diffractometer (D8 Advance, Bruker, Germany) equipped with filtered Cu-*Kα* radiation ($\lambda = 1.5418$ Å) by step scanning with an interval of 0.02° in the 2θ range of 20°–80°. SEM images were obtained on a field-emission scanning electron microscope (FEI Nova Nano-SEM 450). HRTEM image were obtained using FEI Tecnai G2 F20 operating at 200 kV. STEM image and elemental mapping images were obtained using Tecnai F20 SuperTwin operating at 200 kV. Nitrogen sorption isotherms were measured at 77 K with a Micromeritic Tri Flex surface characterization analyzer and the specific surface areas were calculated by using the BET method. EPR spectra were obtained at a Bruker EPR A300 spectrometer. UV–vis spectra were analyzed by UV-2600 UV–Vis Spectrophotometers (Shimadzu) with $BaSO_4$ as the internal reflectance standard. XPS experiments were carried out on the Nexsa surface analysis system with Al *Kα* X-ray source for radiation and data were fitted by the public software package XPSPEAK. XAS measurements were performed at the soft X-ray spectroscopy beamline of the Australian Synchrotron. The XAS measurements at the O-*K* edge and Fe-*L* edge were performed in total electron yield mode using linearly polarized X-rays, and the photon energy was calibrated using spectra from pre-calibrated reference foils.

2.3. Electrode preparation

Working electrodes for OER tests were prepared by a controlled drop-casting method on a RDE (Pine Research Instrumentation, 5 mm diameter). The RDE was pre-polished with aqueous alumina suspension on a polishing cloth. To eliminate the electrode conductivity restriction within thin film working electrodes, the catalysts in this work were mixed with as-obtained conductive carbon (Super P Li) at a mass ration of 1:1. Briefly, a 5 μL aliquot of the catalyst ink, which was prepared by sonication of a mixture of 10 mg of oxide powder and 10 mg of conductive carbon dispersed in 1 mL ethanol and 100 μL of 5 wt% Nafion solution for at least 1 h, was dropped on the electrode surface, generating an approximate catalyst loading of 0.464 mg_{total} cm^{-2} (0.232 mg_{oxide} cm^{-2}) and was left to dry before the electrochemical tests.

2.4. Electrochemical measurements

OER activity in 0.1 M KOH solution was conducted using in a standard three-electrode electrochemical cell (Pine Research Instrumentation) with an RDE configuration controlled by a CHI 760E electrochemistry workstation. Catalysts cast on RDE, Pt foil and Ag|AgCl (3.5 M KCl) were used as the working electrode, counter electrode, and reference electrode, respectively. During the measurement, RDE electrode was constantly rotating at 1600 rpm to get rid of the bubbles. The electrolyte was bubbled with O_2 for ~30 min prior to OER measurements and maintained under O_2 atmosphere throughout the test period. OER polarization curves were collected by capacitance-corrected cyclic voltammetry (CV) curves at a scan rate of 10 mV s^{-1} from 0.2 to 1 V vs. Ag|AgCl. Polarization curves were *iR* corrected in this work unless noted otherwise. The polarization curves were replotted as overpotential (η) versus the logarithm of current density (log $|J|$) to obtain Tafel plots.

2.5. Computational methods

The spin-polarized density functional theory (DFT) calculations were carried out using Vienna *ab initio* simulation package (VASP) within the projected-augmented wave method [39,40]. We used the revised Perdew-Burke-Ernzerhof (PBE) functional with the Hubbard U values of 5.3 eV for Fe [41,42]. The plane wave energy cutoff was 400 eV. The electronic energy and force convergence criteria were 10^{-5} eV and 0.05 eV/Å, respectively. A 2 × 2 × 2 supercell (160-atoms) was adopted to simulate the low chlorine doping concentration. The density of states (DOS) were computed with *k*-points mesh of 3 × 3 × 2.

3. Results and discussion

Parent $LaFeO_3$ (LFO) and Cl-doped $LaFeO_{2.9-\delta}Cl_{0.1}$ (LFOCl) perovskites were synthesized by a combined ethylenediaminetetraacetic acid-citric acid (EDTA-CA) complexing sol-gel method (see the detailed synthesis process in experimental section). Fig. 1(a) shows the X-ray diffraction (XRD) patterns of as-prepared LFO and LFOCl powders. As observed, both samples exhibit a pure orthorhombic perovskite structure with a space group of Pnma (JCPDS, No 88–0641) [23]. The XRD main peak of LFOCl shifts slightly to lower angles as compared with that of the parent LFO, implying a lattice expansion after the Cl doping due to the substitution of smaller O^{2-} (1.40 Å) by larger Cl^- ion (1.81 Å). The phase structure of LFOCl was further confirmed by the high-resolution transmission electron microscope (HRTEM). A lattice fringe with interplanar distances of 0.28 nm was observed, corresponding to the (121) crystal planes of orthorhombic LFOCl (Fig. 1(b)). The X-ray photoelectron spectroscopy (XPS) spectrum of LFOCl in Fig. 1(c)

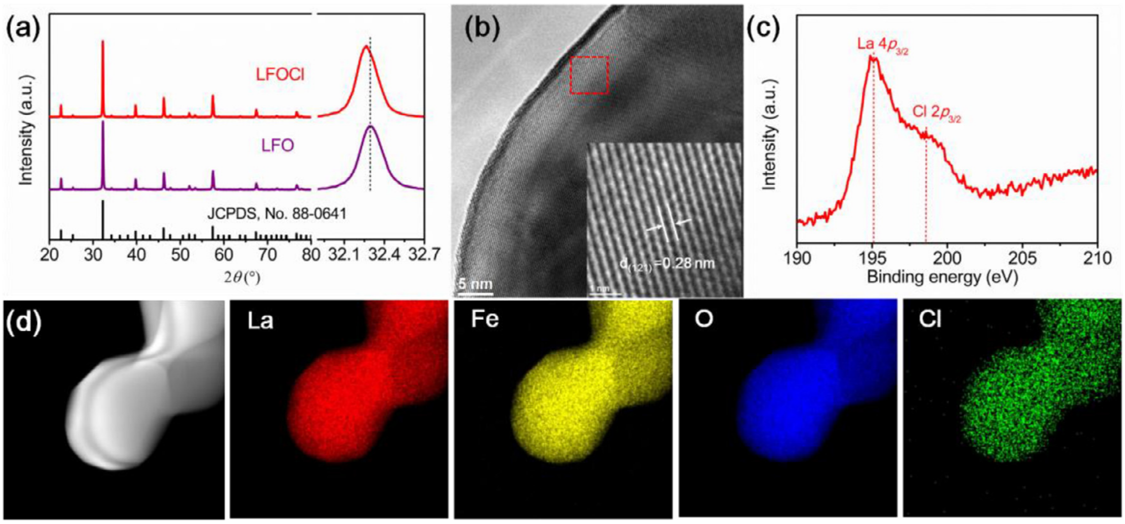

Fig. 1. (a) XRD patterns of LFO and LFOCl. (b) HRTEM image of LFOCl. (c) XPS spectra of La 4*p* & Cl 2*p* for LFOCl. (d) HAADF-STEM image and the corresponding elemental mapping images of LFOCl.

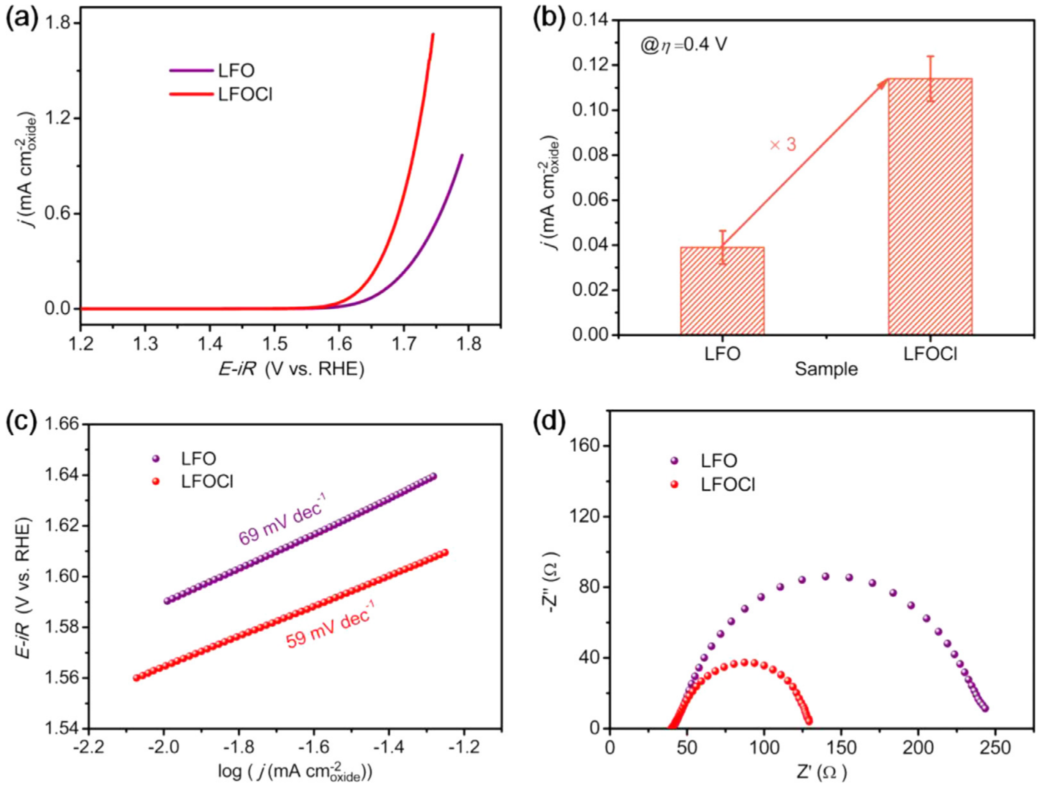

Fig. 2. (a) Capacitance- and ohmic resistance-corrected polarization curves of LFO and LFOCl catalysts in O_2-saturated 0.1 M KOH solution, with OER current normalized to the BET surface area. (b) Specific activity of LFO and LFOCl catalysts at $\eta = 0.4$ V. The error bars represent standard deviations from at least three independent measurements. (c) Tafel plots derived from the data shown in (a). (d) Nyquist plots of LFO and LFOCl catalysts recorded at 0.7 V vs. Ag/AgCl (no *iR*-corrected) under the influence of an AC voltage of 10 mV.

displays a peak at a binding energy of ~198.5 eV, which can be assigned to the Cl $2p_{3/2}$ signal, confirming the presence of Cl^- in LFOCl. Moreover, the high-angle annular dark-field scanning transmission electron microscopy (HAADF-STEM) and elemental mapping images (Fig. 1(d)) demonstrate the homogeneous distribution of La, Fe, O and Cl elements in the as-prepared LFOCl sample. The energy dispersive X-ray (EDX) analysis reveal an approximate 0.99:1.00:2.79:0.08 atomic ratio for La:Fe:O:Cl, which is close to the intended compositions (Table S1). The morphology was examined by scanning electron microscopy (SEM). It can be seen that some nanometer-sized particles are agglomerated into similar chunks in both LFO and LFOCl samples (Fig. S1).

The OER activity of LFO and LFOCl perovskites was evaluated by a thin-film rotating disk electrode (RDE) technique [8]. All potential data in this work were corrected to reversible hydrogen electrode (RHE, Fig. S2), and the polarization curves were obtained by taking an average of forward and backward cyclic voltammetry (CV) curves (Fig. S3) [8]. Fig. S4 and Fig. 2(a) present the capacitance-

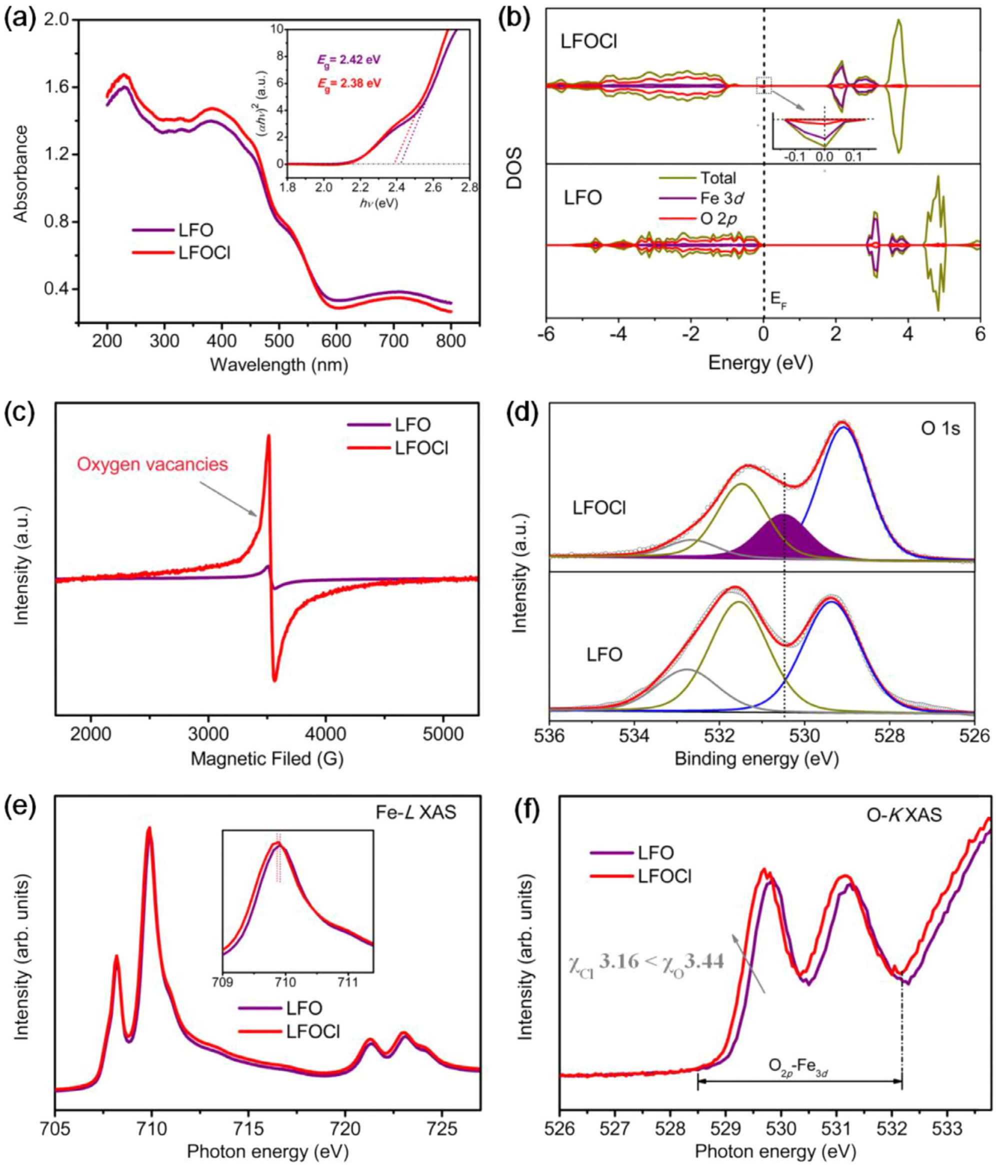

Fig. 3. (a) UV–vis absorption spectra of LFO and LFOCl. Inset is the corresponding Tauc plots. (b) DOS profiles of LFO and LFOCl. Inset is the magnified zone. (c) EPR spectra of LFO and LFOCl. (d) XPS spectra of O 1*s* species on the surface of LFO and LFOCl. (e) The Fe-*L* sXAS spectra of LFO and LFOCl. Inset is the magnified part. (f) The O-*K* sXAS spectra LFO and LFOCl.

and *iR*-corrected polarization curves of LFO and LFOCl in 0.1 M KOH solution, where current values were normalized to the electrode geometric area and Brunauer-Emmett-Teller (BET) surface area of perovskites (Fig. S5 and Table S2), respectively. The LFOCl exhibits evidently smaller onset overpotential (defined here as the overpotential at 1 mA cm^{-2}) and larger specific catalytic current than parent LFO, suggesting much better OER activity of LFOCl. The overpotential at 10 mA cm^{-2} of LFOCl is ~0.46 V, also much lower than that (~0.51) of LFO. Besides, the specific activity of LFO is signficnatly enahnced after proper Cl-anion doping. For example, the specific activity of LFOCl at η=0.4 V is 0.114 mA cm^{-2}, which is ~3-fold higher than that of parent LFO (Fig. 2(b)), indicative of the significant intrinsic activity enhancemen after Cl doping. To examine the kinetics of OER, Tafel plots were drawn in Fig. 2(c). The Tafel slope for LFOCl (59 mV dec^{-1}) is smaller than that for LFO (69 mV dec^{-1}), implying faster OER rates. Electrochemical impedance spectroscopy (EIS) measurements were further performed to explore the kinetics during the OER process. Nyquist plots shown in Fig. 2(d) reveal that the LFOCl possesses a much smaller charge transfer resistance than LFO, demonstrating that the Cl dopant could promote charge transfer during the OER, due presumably to the increased electrical conductivity of LFOCl as will be discussed below. In addition, what is noteworthy is that the Cl doping for O site in $LaFeO_{3\text{-}x\text{-}\delta}Cl_x$ (x = 0, 0.05, 0.1, 0.2) generates a volcano-like activity trend with ~3.3% Cl dopant (i.e., x = 0.1 for LFOCl) being the highest (Figs. S3 and S4). The OER performance of LFOCl is comparable to those of the benchmark IrO_2 (Fig. S8) and some state-of-the-art perovskite electrocatalysts ever reported (Table S3).

Above electrochemical analysis indicates that the Cl-anion doping into LFO can significantly enhance the OER activity, which can mainly be ascribed to the following beneficial factors. First, Cl doping results in the increased electrical conductivity. It is known that electrocatalysis process requires an efficient flow of electrons through the electrode to produce high current; therefore, high electrical conductivity would expedite the charge transfer rate of the catalyst and benefit the high-efficiency catalysis [12,29,35,43,44]. The electronic behavior was firstly explored by the UV–vis absorption spectra, and the corresponding optical band

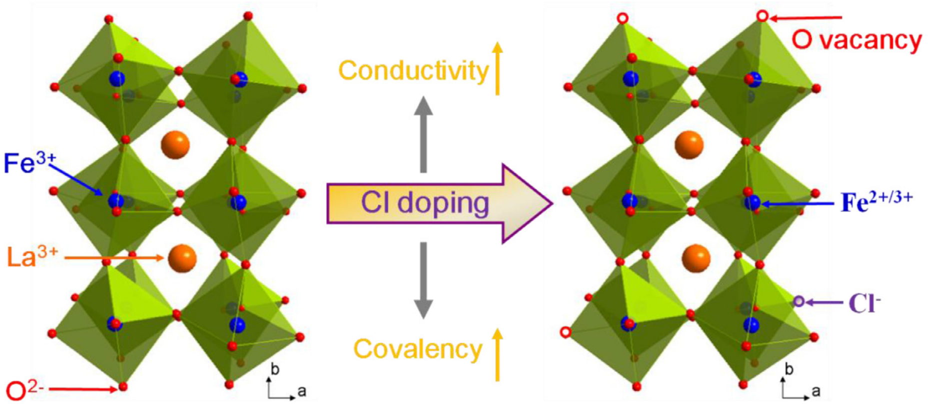

Fig. 4. Schematic illustration of Cl-doping-induced multiple beneficial factors in LFO perovskite for boosting OER.

gaps were calculated according to the Tauc equation (Fig. 3(a)). The band gap of parent LFO narrows from 2.42 eV to 2.38 eV after Cl doping, which benefits the excitation of charge carriers to the conduction band and consequently lead to enhanced electrical conductivity of LFOCl. We also use density functional theory (DFT) calculations to unveil the electronic properties of LFO and LFOCl by calculating the density of states (DOS). As can be seen in Fig. 3(b), the parent LFO is a typical semiconducor with a large bandgap. Nevertheless, an evident Fe 3*d* orbital crossing the Fermi level was observed for LFOCl, accounting for the increased conductivity after Cl doping. Second, abundant oxygen vacancies are created after Cl doping. The oxygen vacancies formation after Cl doping was detected by the electron paramagnetic resonance (EPR) and X-ray photoelectron spectroscopy (XPS) techniques. EPR spectra are sensitive to unpaired electrons trapped by oxygen vacancies [12,19]. LFOCl exhibits a strong signal intensity at $g = 2.003$ while LFO has a very weak signal (Fig. 3(c)), revealing much higher concentration of oxygen vacancies in LFOCl. Fig. 3(d) shows the O 1*s* XPS spectra of LFO and LFOCl, which can be fitted by a combination of four characteristic sub-peaks [12,23,27,28,30]. Based on the deconvolution results (Table S2), a much larger number of (O_2^{2-}/O^-) species, which is closely related to the surface oxygen vacancies [23,27,45,46], was formed on the surface of LFOCl. Previous studies have widely reported that introducing oxygen vacancies on metal oxides can effectively promote the OER catalysis [23,26,35,47–49]. It is reasonable to believe that rich oxygen deficiencies, as induced by the Cl doping, are crucial to the enhanced OER activity of LFOCl. Third, Cl doping contributes to the enhanced Fe-O covalency. The significance of the metal-oxygen covalency was highlighted by some recent studies about transition metal oxides involving lattice-oxygen-redox during OER catalysis [6,7,50–55]. Specially, the strong covalency between metal and oxygen ions can trigger lattice-oxygen activation for OER, which potentially offers better OER activity [50–53]. Surface-sensitive soft X-ray absorption spectroscopy (sXAS) technique was employed to study the electronic structures. The Fe *L*-edge peak of LFOCl slightly shifts to lower energies compared to parent LFO (Fig. 3(e)), suggesting slight decreased Fe valence state possibly arising from the generation of oxygen vacancy conforming to charge neutrality. O *K*-edge XAS spectra can directly reflect the metal 3*d*-oxygen 2*p* covalency because the pre-edge peak below ~532 eV represents the unoccupied O 2*p* orbitals hybridized with transition metal 3*d* orbitals [55–57]. As displayed in Fig. 3(f), lower pre-edge energy position and higher intensity of the pre-edge peak in LFOCl were observed relative to parent LFO, demonstrating the enhanced Fe-O covalency. The enhanced Fe-O covalency after Cl doping could be understood from lower electronegativity of Cl over O (3.16 vs. 3.44), as Cl is less capable than O of attracting electrons from Fe ions [31,58]. To sum up, all aforementioned beneficial factors (i.e., increased oxygen vacancies, conductivity and covalency) schematically shown in Fig. 4 is responsible for the significantly enhanced OER intrinsic activity of Cl doped LFOCl perovskite.

4. Conclusions

In summary, we have demonstrated a chlorine (Cl)-anion doping strategy to induce multi-factor optimization of perovsktie oxides toward boosted OER electrocatalysis. A representative parent perovskite $LaFeO_3$ (LFO) was selected as a proof-of-concept to study the effect of Cl-doping on the OER activity. Specifically, $LaFeO_{2.9-\delta}Cl_{0.1}$ (LFOCl) shows an approximately threefold increase in intrinsic OER activity as compared with the parent LFO. The intrinsic activity enhancement is resulted from the Cl dopant, endowing LFOCl with multiple beneficial factors for catalyzing OER such as rich oxygen vacancies, increased electrical conductivity and enhanced Fe-O covalency. Our study not only reports an efficient OER electrocatalyst, but also opens up a new avenue to develop other advanced catalysts for energy-related applications.

Declaration of Competing Interest

The authors declare that they have no known competing financial interests or personal relationships that could have appeared to influence the work reported in this paper.

Acknowledgments

This work was financially supported by the Australian Research Council (Discovery Early Career Researcher Award No. DE190100005). The authors acknowledge Monash X-Ray Platform (MXP). Dr. D. Qi. acknowledges the support of the Australian Research Council (Grant No. FT160100207) and the ontinued support from the Queensland University of Technology (QUT) through the centre for Materials Science. Part of this research was undertaken on the Soft X-ray Spectroscopy beamline at the Australian Synchrotron, part of ANSTO.

Supplementary materials

Supplementary material associated with this article can be found, in the online version, at doi:10.1016/j.jechem.2020.03.055.

References

[1] S. Chu, A. Majumdar, Nature 488 (2012) 294–303.

[2] Z.W. Seh, J. Kibsgaard, C.F. Dickens, I. Chorkendorff, J.K. Nørskov, T.F. Jaramillo, Science 355 (2017) eaad4998.
[3] D. Chen, C. Chen, Z.M. Baiyee, Z. Shao, F. Ciucci, Chem. Rev. 115 (2015) 9869–9921.
[4] X. Deng, J. Huang, H. Wan, F. Chen, Y. Lin, X. Xu, R. Ma, T. Sasaki, J. Energy Chem. 32 (2019) 93–104.
[5] W. Zhang, D. Li, L. Zhang, X. She, D. Yang, J. Energy Chem. 39 (2019) 39–53.
[6] Y. Zhu, H.A. Tahini, Z. Hu, Y. Yin, Q. Lin, H. Sun, Y. Zhong, Y. Chen, F. Zhang, H.-J. Lin, C.-T. Chen, W. Zhou, X. Zhang, S.C. Smith, Z. Shao, H. Wang, EcoMat (2020) DOI: 10.1002/eom2.12021.
[7] Y. Zhu, H.A. Tahini, Z. Hu, Z.G. Chen, W. Zhou, A.C. Komarek, Q. Lin, H.-J. Lin, C.-T. Chen, Y. Zhong, M.T. Fernández, S.C. Smith, H. Wang, M. Liu, Z. Shao, Adv. Mater. 32 (2020) 1905025.
[8] J. Suntivich, K.J. May, H.A. Gasteiger, J.B. Goodenough, Y. Shao-Horn, Science 334 (2011) 1383–1385.
[9] X. Li, H. Wang, Z. Cui, Y. Li, S. Xin, J. Zhou, Y. Long, C. Jin, J.B. Goodenough, Sci. Adv. 5 (2019) eaav6262.
[10] Y. Zhu, W. Zhou, Z. Chen, Y. Chen, C. Su, M.O. Tadé, Z. Shao, Angew. Chem. Int. Ed. 54 (2015) 3897–3901.
[11] S. Yagi, I. Yamada, H. Tsukasaki, A. Seno, M. Murakami, H. Fujii, H. Chen, N. Umezawa, H. Abe, N. Nishiyama, S. Mori, Nat. Commun. 6 (2015) 8249.
[12] J. Dai, Y. Zhu, Y. Yin, H.A. Tahini, D. Guan, F. Dong, Q. Lu, S.C. Smith, X. Zhang, H. Wang, W. Zhou, Z. Shao, Small 15 (2019) 1903120.
[13] Q. Lin, Y. Zhu, Z. Hu, Y. Yin, H.-J. Lin, C.-T. Chen, X. Zhang, Z. Shao, H. Wang, J. Mater. Chem. A. 8 (2020) 6480–6486, doi:10.1039/c9ta13972a.
[14] B. Li, Z. Xia, B. Zhang, C. Tang, H. Wang, Q. Zhang, Nat. Commun. 8 (2017) 934.
[15] B. Li, C. Tang, H. Wang, X. Zhu, Q. Zhang, Sci. Adv. 2 (2016) e1600495.
[16] Y. Wei, J. Liu, Z. Zhao, Y. Chen, C. Xu, A. Duan, G. Jiang, H. He, Angew. Chem., Int. Ed. 50 (2011) 2326–2329.
[17] W. Wan, R. Tran, J. Qu, Y. Liu, C. Chen, M. Xu, Y. Chen, S.P. Ong, L. Wang, W. Zhou, Z. Shao, ACS Appl. Mater. Interf. 11 (2019) 35641–35652.
[18] M.M. Natile, A. Ponzoni, I. Concina, A. Glisenti, Chem. Mater. 26 (2014) 1505–1513.
[19] J. Li, J. Miao, X. Duan, J. Dai, Q. Liu, S. Wang, W. Zhou, Z. Shao, Adv. Funct. Mater. 28 (2018) 1804654.
[20] E. Maguire, B. Gharbage, F.M.B. Marques, J.A. Labrincha, Solid State Ionics 127 (2000) 329–335.
[21] Y.-L. Lee, M.J. Gadre, Y. Shao-Horn, D. Morgan, Phys. Chem. Chem. Phys. 17 (2015) 21643–21663.
[22] J. Sunarso, A.A. Torriero, W. Zhou, P.C. Howlett, M. Forsyth, J. Phys. Chem. C 116 (2012) 5827–5834.
[23] Y. Zhu, W. Zhou, J. Yu, Y. Chen, M. Liu, Z. Shao, Chem. Mater. 28 (2016) 1691–1697.
[24] J. Xu, Z. Wang, D. Xu, F. Meng, X. Zhang, Energy Environ. Sci. 7 (2014) 2213–2219.
[25] Z. Shen, Y. Zhuang, W. Li, X. Huang, F.E. Oropeza, E.J.M. Hensen, J.P. Hofmann, M. Cui, A. Tadich, D. Qi, J. Cheng, J. Li, K.H.L. Zhang, J. Mater. Chem. A 8 (2020) 4407–4415.
[26] S. She, J. Yu, W. Tang, Y. Zhu, Y. Chen, J. Sunarso, W. Zhou, Z. Shao, ACS Appl. Mater. Interf. 10 (2018) 11715–11721.
[27] J. Dai, Y. Zhu, Y. Zhong, J. Miao, B. Lin, W. Zhou, Z. Shao, Adv. Mater. Interf. 6 (2019) 1801317.
[28] Z. Li, L. Lv, J. Wang, X. Ao, Y. Ruan, D. Zha, G. Hong, Q. Wu, Y. Lan, C. Wang, J. Jiang, M. Liu, Nano Energy 47 (2018) 199–209.
[29] W. Wang, Y. Yang, D. Huan, L. Wang, N. Shi, Y. Xie, C. Xia, R. Peng, Y. Lu, J. Mater. Chem. A 7 (2019) 12538–12546.
[30] J. Xiong, H. Zhong, J. Li, X. Zhang, J. Shi, W. Cai, K. Qu, C. Zhu, Z. Yang, S.P. Beckman, H. Cheng, Appl. Catal. B: Environ. 256 (2019) 117817.
[31] B. Hua, M. Li, W. Pang, W. Tang, S. Zhao, Z. Jin, Y. Zeng, B.S. Amirkhiz, J.L. Luo, Chem 4 (2018) 2902–2916.
[32] Z. Zhang, Y. Zhu, Y. Zhong, W. Zhou, Z. Shao, Adv. Energy Mater. 7 (2017) 1700242.
[33] Y. Li, Y. Li, Y. Wan, Y. Xie, J. Zhu, H. Pan, X. Zheng, C. Xia, Adv. Energy Mater. 9 (2019) 1803156.
[34] J. Zhu, G. Liu, Z. Liu, Z. Chu, W. Jin, N. Xu, Adv. Mater. 28 (2016) 3511–3515.
[35] S. Peng, X. Han, L. Li, S. Chou, D. Ji, H. Huang, Y. Du, J. Liu, S. Ramakrishna, Adv. Energy Mater. 8 (2018) 1800612.
[36] Y. Liu, W. Wang, X. Xu, J.-P.M. Veder, Z. Shao, J. Mater. Chem. A 7 (2019) 7280–7300.
[37] H. Wang, C. Tang, B. Wang, B. Li, Q. Zhang, Adv. Mater. 29 (2017) 1702327.
[38] J. Zhang, Y. Cui, L. Jia, B. He, K. Zhang, L. Zhao, Int. J. Hydrog. Energy 44 (2019) 24077–24085.
[39] G. Kresse, J. Furthmüller, Phys. Rev. B 54 (1996) 11169–11186.
[40] P.B. Blochl, Phys. Rev. B 50 (1994) 179523-17979.
[41] B. ammer, L.B. Hansen, J.K. Nørskov, Phys. Rev. B 59 (1999) 7413.
[42] S.L. Dudarev, G.A. Botton, S.Y. Savrasov, C.J. Humphreys, A.P. Sutton, Phys. Rev. B 57 (1998) 1505.
[43] Y. Zhu, W. Zhou, Z. Shao, Small 13 (2017) 1603793.
[44] Y. Zhu, H.A. Tahini, Z. Hu, J. Dai, Y. Chen, H. Sun, W. Zhou, M. Liu, S.C. Smith, H. Wang, Z. Shao, Nat. Commun. 10 (2019) 149.
[45] N.A. Merino, B.P. Barbero, P. Eloy, L.E. Cadús, Appl. Surf. Sci. 253 (2006) 1489–1493.
[46] J. Zhu, H. Li, L. Zhong, P. Xiao, X. Xu, X. Yang, Z. Zhao, J. Li, ACS Catal 4 (2014) 2917–2940.
[47] J. Bao, X. Zhang, B. Fan, J. Zhang, M. Zhou, W. Yang, X. Hu, H. Wang, B. Pan, Y. Xie, Angew. Chem. Int. Ed. 54 (2015) 7399–7404.
[48] S. Hirai, K. Morita, K. Yasuoka, T. Shibuya, Y. Tojo, Y. Kamihara, A. Miura, H. Suzuki, T. Ohno, T. Matsuda, S. Yagi, J. Mater. Chem. A 6 (2018) 15102–15109.
[49] J. Du, T. Zhang, F. Cheng, W. Chu, Z. Wu, J. Chen, Inorg. Chem. 253 (2014) 9106–9114.
[50] A. Grimaud, O. Diaz-Morales, B. Han, W.T. Hong, Y.L. Lee, L. Giordano, K.A. Stoerzinger, M.T. Koper, Y. Shao-Horn, Nat. Chem. 9 (2017) 457–465.
[51] J.T. Mefford, X. Rong, A.M. Abakumov, W.G. Hardin, S. Dai, A.M. Kolpak, K.P. Johnston, K.J. Stevenson, Nat. Commun. 7 (2016) 11053.
[52] Z. Huang, J. Song, Y. Du, S. Xi, S. Dou, J.M.V. Nsanzimana, C. Wang, Z.J. Xu, X. Wang, Nat. Energy 4 (2019) 329–338.
[53] J.S. Yoo, X. Rong, Y. Liu, A.M. Kolpak, ACS Catal. 8 (2018) 4628–4636.
[54] Y. Duan, S. Sun, S. Xi, X. Ren, Y. Zhou, G. Zhang, H. Yang, Y. Du, Z. Xu, Chem. Mater. 29 (2017) 10534–10541.
[55] J. Liu, E. Jia, L. Wang, K.A. Stoerzinger, H. Zhou, C.S. Tang, X. Yin, X. He, E. Bousquet, M.E. Bowden, A.T.S. Wee, S.A. Chambers, Y. Du, Adv. Sci. 6 (2019) 1901073.
[56] X. Wang, Z. Pan, X. Chu, K. Huang, Y. Cong, R. Cao, R. Sarangi, L. Li, G. Li, S. Feng, Angew. Chem. Int. Ed. 131 (2019) 11846–11851.
[57] C. Shang, C. Cao, D. Yu, Y. Yan, Y. Lin, H. Li, T. Zheng, X. Yan, W. Yu, S. Zhou, J. Zeng, Adv. Mater. 31 (2019) 1805104.
[58] S. Sun, Y. Sun, Y. Zhou, S. Xi, X. Ren, B. Huang, H. Liao, L.P. Wang, Y. Du, Z. Xu, Angew. Chem. Int. Ed. 131 (2019) 6103–6108.